Atomic size-limited intercalation into single wall carbon nanotubes

2007 Nanotechnology 18 435705

(http://iopscience.iop.org/0957-4484/18/43/435705)

IOP PUBLISHING NANOTECHNOLOGY
Nanotechnology **18** (2007) 435705 (5pp) doi:10.1088/0957-4484/18/43/435705

Atomic size-limited intercalation into single wall carbon nanotubes

L Grigorian[1,4], S Colbern[1], I O Maciel[2], M A Pimenta[2], F Plentz[2] and A Jorio[2,3]

[1] YTC America Incorporated, Camarillo, CA 93012, USA
[2] Departamento de Física, Universidade Federal de Minas Gerais, CEP 30123-970, Belo Horizonte, MG, Brazil
[3] Materials Metrology Division, Brazilian National Institute of Metrology, Xerém-Duque de Caxias, RJ, Brazil

E-mail: lgrigorian@ytca.com

Received 15 August 2007, in final form 31 August 2007
Published 4 October 2007
Online at stacks.iop.org/Nano/18/435705

Abstract
Intercalation of single wall carbon nanotubes (SWNTs) provides an important tool to modify their electronic band structure. Using multiple excitation wavelength Raman spectroscopy, we demonstrate that intercalation into SWNT interiors can be limited by intercalant size resulting in an unusual material comprising SWNTs with varying charge density. In the particular case of iodine intercalation, larger SWNTs with iodine-filled interiors were found to carry significantly higher charge density as compared to smaller empty ones. This difference was used to separate the intercalated SWNT material into fractions with homogeneous charge density.

1. Introduction

A remarkable feature of single wall carbon nanotubes (SWNTs) is their small diameter approaching the size of individual atoms. For example, commercial CoMoCat material (available from SouthWest NanoTechnologies, http://www.swnano.com) comprises predominantly (6, 5) and (7, 5) nanotubes with diameters $d = 0.757$ and 0.829 nm, respectively [1]. Taking into account nanotube wall thickness (∼0.350 nm [2]), the inner diameters d_{in} are 0.407 and 0.479 nm, respectively. These values are comparable to the diameters of large ions such as iodine ($d_I = 0.432$ nm), i.e., $d_{in}(6, 5) < d_I < d_{in}(7, 5)$. Here, we demonstrate experimentally that intercalation into the interior of SWNTs can be limited by the size of the intercalant atoms resulting in a highly uneven distribution of intercalant-transferred charge among the tubes. In particular, larger nanotubes ($d_{in} > d_I$) with iodine-filled interiors, e.g., (7, 5) were found to carry a significantly higher charge density as compared to smaller ($d_{in} < d_I$) empty ones, e.g., (6, 5). This resulted in an unusual material comprising nanotubes with varying charge density.

Control over the electronic band structure and the Fermi level are important for various potential applications of SWNTs, e.g., in electronics. The SWNT band structure can be modified by intercalating with various molecular and atomic species such as halogens [2–5], alkali metals [5], metal halides, oxides, etc [6]. There are two sites accessible for intercalant species: interstitial channels within bundles and the SWNT interior. In particular, intercalated iodine was found to form negatively charged polyiodide chains, $(I_3)^-$ and $(I_5)^-$, residing both outside and inside positively charged SWNTs [2–4]. The diameters of the SWNTs used in these experiments were typically relatively large ($d > 1.2$ nm and $d_{in} > 0.85$ nm), providing ample room to accommodate the intercalated species inside these nanotubes.

However, atomic size limitations become prominent when smaller diameter nanotubes (such as CoMoCat) are used as hosts for intercalation. With respect to iodine, these nanotubes fall into one of two categories depending on their diameter: in the larger ($d_{in} > d_I$) tubes, iodine ions can reside both outside and inside nanotubes, whereas the smaller ($d_{in} < d_I$) tubes can accept iodine only at the outside site (figure 1). The first type (figure 1(a)) has more iodine and therefore is expected to carry more positive charge per carbon atom as compared to the second type (figure 1(b)). Hence, intercalated CoMoCat material would comprise two subsets of nanotubes with two distinct values of charge density.

[4] Author to whom any correspondence should be addressed.

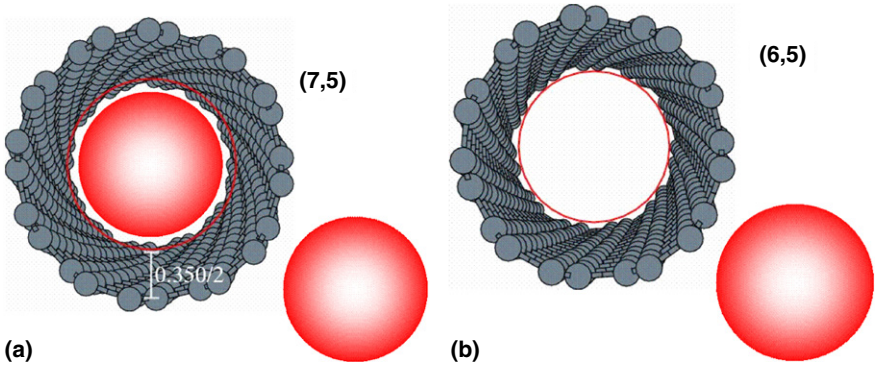

Figure 1. Two types of intercalated SWNTs: (a) the larger diameter tubes, as represented by (7, 5), and (b) the smaller diameter tubes, as represented by (6, 5). The drawings are roughly to scale. The red circles represent the inner diameter as defined by the pi-electronic cloud extending $0.350/2 = 0.175$ nm from each side of the nanotube walls. The intercalated iodine ions are shown as red spheres.

This unusual situation is not easily revealed experimentally as tubes of both types coexist randomly in bundles resulting in averaged charge density. In order to clearly demonstrate the uneven charge density distribution, the intercalated sample should be separated into fractions enriched with (7, 5) and (6, 5) tubes (representing the first and second types, respectively). Owing to the different charge densities, these two types interact with different strength with ionic surfactants, and this can be used to separate them into two distinct fractions. This defines our approach: (1) intercalate iodine into CoMoCat nanotubes, (2) separate the intercalated sample into two fractions enriched with the first and second type of nanotubes, (3) characterize the separated fractions to assess the enrichment, and (4) demonstrate that the fractions carry significantly different charge per carbon atom.

2. Experimental details

2.1. Intercalation and separation procedures

The separation procedure included several steps. First, the starting SWNT was intercalated with iodine. Second, the reaction product was annealed to remove unreacted iodine. Third, the annealed powder was dispersed in de-ionized water and centrifuged at high speed. Finally, the supernatant (SN) and precipitate (PP) fractions were separated and dried.

In the first step, 20 mg of purified CoMoCat SWNT material was degassed in the reaction chamber by heating to 140 °C in vacuum (1 Torr) for 20 min. Next, the vacuum pump was disconnected, and the reaction was carried out by adding iodine powder (10 g) and heating the mixture at 150 °C for 30 min. Then, the temperature was decreased to 100 °C and the vacuum pump was connected again (1 Torr) to remove the excess, unreacted iodine. Weight uptake measurements yielded an IC_{12} final composition consistent with that reported in the literature [3].

The intercalated IC_{12} powder was suspended in water using CTAB (cetyltrimethylammonium bromide) as a surfactant and dispersed by high shear mixing using a Microfluidics microfluidizer processor (www.microfluidicscorp.com) model M110Y (total of 22 passes at 26.5 kPSI pressure), then centrifuged at 20 000g (Fisher 21000R) for 4 h. The resulting supernatant was carefully separated from the precipitate fraction by decanting. Both fractions were consequently annealed in vacuum ($\sim 10^{-2}$ Torr) at 500 °C for 4 h to remove all intercalated iodine and surfactant and regenerate pure SWNTs. This was necessary to facilitate Raman characterization of the separated fractions as the intercalation has a strong impact on the resonance conditions of individual nanotubes. Complete iodine removal was confirmed by Raman spectra (as judged by the disappearance of the polyiodide peaks at e.g., 109, 130, 148 cm^{-1}, as well as a down-shift of the G-bands to their initial positions before iodine intercalation) and energy-dispersive x-ray (EDX) spectra.

2.2. Resonance Raman and photoluminescence (PL) spectroscopy

Raman spectra were measured using a Dilor XY triple-monochromator equipped with a N_2-cooled charge coupled device (CCD) detector. Measurements were performed in a backscattering configuration with an 80× microscope objective lens. The results obtained earlier for starting CoMoCat material [9] provided a guide on selecting several specific excitation wavelengths to cover all major SWNT species. As excitation sources we used six specially selected laser lines from an ArKr and ten specially selected excitation laser lines from a dye laser, pumped by a 6 W Ar laser, using the DCM Special in the range from 654.5 nm (1.90 eV) to 612.1 nm (2.03 eV), and the Rhodamine 6G dyes in the range from 605.0 nm (2.05 eV) to 567.9 nm (2.18 eV). The six ArKr laser lines were 647 nm (1.92 eV), 568 nm (2.18 eV), 514.5 nm (2.41 eV), 488 nm (2.54 eV), 476.5 nm (2.60 eV), and 457.9 nm (2.71 eV).

The 532 nm excitation wavelength spectra were measured using a Horiba Jobin Yvon Aramis Raman spectrometer. The spectrometers were calibrated for absolute intensity. For frequency adjustments, the spectrometer was calibrated during the measurement procedure, every time the excitation laser energy was changed. In addition, for each laser excitation energy, Si substrate spectra were acquired as a reference. The data were analyzed using the Origin (for visual comparative analysis and figure preparations) and

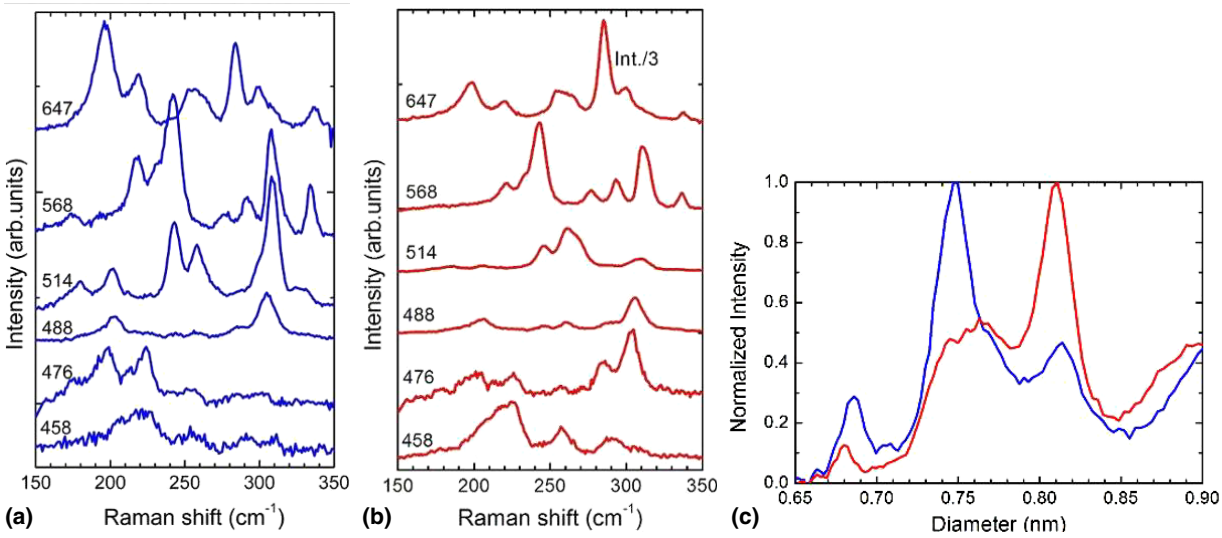

Figure 2. Establishing the separation: Raman radial breathing modes of annealed PP (a), and SN (b) fractions collected with the six shown excitation wavelengths (nm); (c) sum of spectra near the separation boundary. In (c), the blue trace refers to PP, and the red trace to SN fractions.

PeakFit software (for quantitative analysis). In the PeakFit software, the non-Raman related baselines were removed, and the spectra were fitted using a sum of Lorentzians. From the fitting procedure we extracted the radial breathing mode frequencies, linewidths, intensities and integrated areas. Photoluminescence (PL) spectra were measured at 647 nm with a SPEX 750M spectrometer equipped with a 600 l mm^{-1} grating blazed at 1000 nm and a Princeton Instruments OMA V InGaAs linear diode array detector. The excitation laser power was set to 10 mW and focused onto the sample using a 10× Mitutoyo M Plan Apo NIR objective lens with a working distance of 30.5 nm, and emission was collected by the same objective lens in a backscattering configuration.

The spectral resolution of the system was 1 nm. The suspensions for PL and some Raman measurements were prepared by sonicating SWNT powders mixed with CTAB surfactant in de-ionized water (200 mg SWNT and 3 g of CTAB per liter of water). The SWNT diameters cited in this work were calculated as $d = (a_{CC}/\pi)\sqrt{\{3(n^2 + nm + m^2)\}}$, where $a_{CC} = 0.142$ nm is the C–C distance, and $\pi = 3.1415$. The ionic diameter of iodine was adopted from [11].

3. Results and discussion

The efficiency of separation depends critically on dispersing SWNT bundles down to individual nanotubes since only isolated tubes can be separated. Practically, it is very difficult to break down all 100% of the SWNT bundles, so a more realistic expectation is enrichment rather than full separation. To assess any enrichment, the SWNT (n, m) population was fully characterized by a combination of Raman and photoluminescence spectroscopies. Multiple excitation wavelengths were required due to the strongly resonant nature of both SWNT Raman [7] and PL [8] spectra. This approach has been used to quantify the (n, m) population of the starting CoMoCat material and estimate that (6, 5) and (7, 5) nanotubes together account for about 60% of the sample [9].

The SWNT Raman spectra feature two major groups of modes: the radial breathing modes (RBM) from ∼150 to 350 cm^{-1} and the tangential modes (TM) at ∼1600 cm^{-1}. RBM frequencies are inversely proportional to nanotube diameters [7, 9] and can therefore be used to determine diameter distribution in the separated fractions after removal of intercalated iodine. At each excitation wavelength, only a few SWNTs of all those present in the sample are in resonance and contribute to the Raman intensity. Accordingly, the RBMs at each wavelength are different as they represent different SWNTs (figures 2(a), (b)). To obtain a representative RBM intensity distribution over the entire sample, these spectra were added up for each fraction (figure 2(c)). The data in figure 2(c) were converted from RBM frequencies (ω_{RBM}) to SWNT diameter units (d) using the relation $d(\text{nm}) = 218.7/[\omega_{RBM}(\text{cm}^{-1}) - 15.3]$ found to work best for CoMoCat nanotubes [9].

The RBM intensity distributions around the boundary ∼295 cm^{-1} or $d \sim 0.78$ nm clearly demonstrate a diameter-based separation in the fractions (figure 2(c)). In particular, the PP fraction is enriched with $d < 0.78$, and SN with $d > 0.78$ nm SWNTs. Note that the data in figure 2(c) represent both metallic and semiconducting nanotubes, so both these populations exhibit the same boundary between the fractions, i.e., there is no metal–semiconductor separation.

Next, we focus on analyzing individual (n, m) tubes to 'personalize' the boundary and define it with higher accuracy. To that end, resonance profiles were obtained for small diameter semiconducting SWNTs (figures 3(a), (b)). Using these data, relative intensities of each (n, m) tube can be determined under the full resonance condition. Comparison of these relative intensities revealed that (6, 5), (8, 3), and (6, 4) tubes were enriched in the PP, and (7, 5) in the SN fractions.

These results place the 'semiconducting' boundary between (8, 3) and (7, 5) nanotubes with $d = 0.782$ and 0.829 nm, respectively. For metallic nanotubes, the boundary was found to be between (7, 4) and (6, 6) nanotubes enriched in the PP and SN fractions, respectively (figure 3(c)). Taking

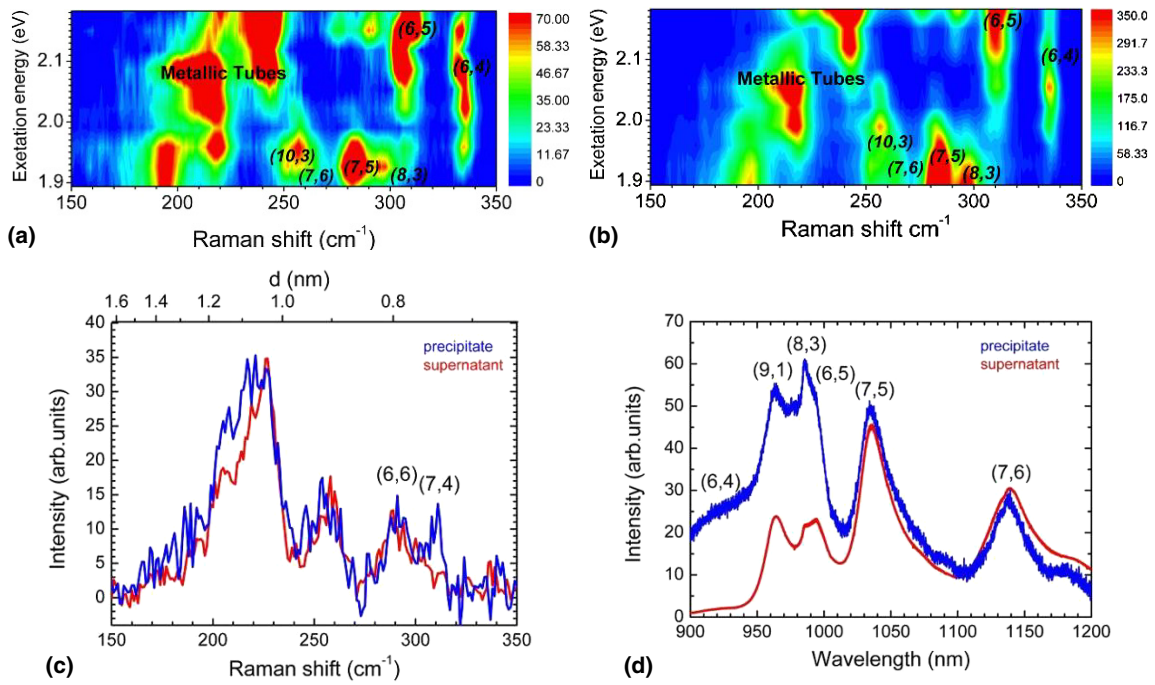

Figure 3. Personalizing the separation boundary: resonance Raman maps for PP (a) and SN (b) fractions in the 1.89–2.18 eV range; (c) 458 nm excitation spectra highlighting the small diameter metallic tubes; (d) PL spectra of the annealed fractions measured with 647 nm excitation. In (a) and (b), RBM resonances for metallic and some semiconducting tubes are marked; colors indicate Raman intensities, as displayed in the intensity bars. Blue and red traces in (c) and (d) represent the PP and SN fractions, respectively.

into account the diameters of these metallic SWNTs, i.e., $d = 0.814$ and 0.755 nm for (6, 6) and (7, 4), respectively, the boundary can be further narrowed down to 32 pm difference between $d(8,\ 3)$ and $d(6,\ 6)$.

Independent verification of Raman data is offered by PL spectra as the Raman and PL cross sections for individual SWNTs are different (figure 3(d)). Enrichment of the PP fraction with (8, 3), (6, 4), and (9, 1) tubes, and the SN fraction with (7, 5) and (7, 6) tubes was clearly observed, consistent with the Raman results.

It should be noted that in the range below 260 cm^{-1}, higher RBM intensities were systematically observed in the PP as compared to the SN fraction (figure 3(c)), indicating that $d > 0.9$ nm tubes went preferentially to the PP fraction. A similar phenomenon was observed earlier for pristine CoMoCat material and was attributed to preferential suspension of smaller diameter tubes by surfactant [9]. The mechanism of this phenomenon is related to the relative size of the SWNT and the surfactant and has nothing to do with iodine intercalation. In the intercalated SWNT samples, both separation mechanisms are superimposed and work independently from each other. This issue is not discussed further in this work as it is unrelated to iodine intercalation.

Summarizing, the combined Raman and PL data provided evidence that SWNTs were separated into two fractions according to their diameters: i.e., $d = 0.782$ nm and smaller tubes went to the PP, and $d = 0.814$ and larger ones to the SN fractions. From these data, the SWNT wall thickness is estimated at 0.350–0.378 nm affording $d = 0.432$ nm iodine ions to fit inside (8, 3) but not (6, 6) tubes. The wall thickness in this sense reflects the space occupied by the pi-electronic cloud

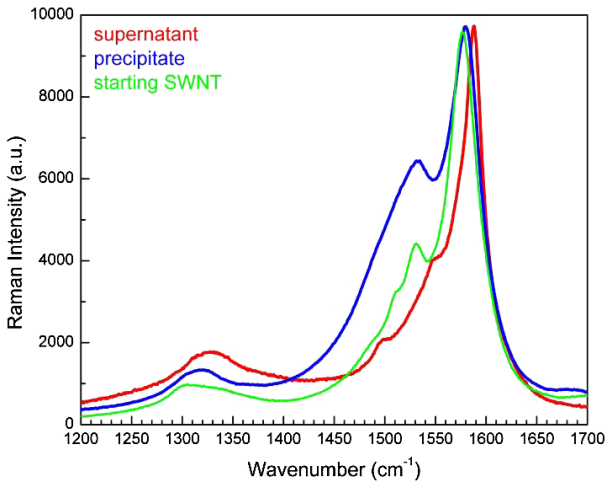

Figure 4. Demonstrating the uneven charge density distribution: Raman spectra (TM range) of the separated fractions before the removal of intercalated iodine (532 nm excitation). The red trace refers to the SN and the blue trace to the PP fractions. The starting SWNT is also shown for reference (green).

that defines the inner opening in the SWNT that is accessible to intercalated species.

Having established that the SN and PP fractions were enriched with the first ($d_{in} > d_I$) and second ($d_{in} < d_I$) type of tubes, respectively, we can now use these fractions to explore the differences in charge density. To that end, we measured Raman spectra of both fractions before the removal of intercalated iodine focusing on TMs that are sensitive to charge distribution within SWNT walls (figure 4). After

intercalation, the TMs up-shifted by 8 cm^{-1} due to contraction of hexagonal carbon rings induced by charge transfer from SWNTs to iodine. The magnitude of the TM up-shift was found to be proportional to the transferred charge density, and in graphite intercalation compounds the TM up-shifts by about 460 cm^{-1} per transferred electron per carbon atom [10]. The observed 8 cm^{-1} up-shift translates into 1 charge per 57.5 carbon atoms, or per 4.8 iodine atoms, consistent with iodine being $(I_3)^-$ and $(I_5)^-$.

In our case, the TMs of the SN and PP fractions were found to be up-shifted by about 11 and 3 cm^{-1} respectively, as compared to the starting SWNT (figure 4), indicating 1 charge per 41.8 and 153 carbon atoms, respectively. Assuming an average of 1 charge per 4.8 iodine atoms, we obtain approximate IC_9 and IC_{32} compositions for the SN and PP fractions, respectively, as compared to the IC_{12} found in the non-separated iodine-intercalated SWNT. This result clearly demonstrates that the SN fraction has significantly (about 3.5 times) more iodine as compared to the PP fraction, and the charge density distribution is very uneven. It should be noted that this number (3.5 times) might not correctly reflect the initial charge density distribution before the separation as some outside iodine could have been lost during the separation process, while more stable interior iodine would have stayed, thereby exaggerating the difference.

Transfer of charge from SWNTs to iodine moves the nanotube Fermi level down into the valence band. One important consequence of varying charge densities would be different positions of Fermi levels of various tubes. The greater the charge transferred per carbon atom, the larger the down-shift of the Fermi levels. At $d > 1.22$ nm, the SWNT interior could accommodate several iodine chains side by side giving rise to even higher charge densities and pushing the SWNT Fermi level further down. The resulting band structure and attending consequences for electronic properties would be complex and non-trivial and have yet to be investigated both experimentally and theoretically. Understanding these consequences would provide insights into fundamental properties as well as new tools to engineer the band structure of nanotube materials.

It is worth noting that this technique can also be used to separate SWNTs according to their diameters. The separation boundary can be adjusted by selecting intercalant species with various diameters and thereby extending this approach to other SWNTs. For example, metal halides where the size of the molecule varies depending on the metal and halogen can be used to separate larger diameter ($d \sim 1.0$–1.5 nm) SWNTs.

In summary, we have demonstrated that intercalation into the interior of SWNTs depends on the size of the intercalant atoms and may lead to a highly uneven distribution of intercalant-transferred charge among the tubes. This difference in charge density was used to separate the intercalated SWNT material into more homogeneous fractions.

Acknowledgments

LG thanks F Kirkbir (YTCA) for useful discussions. The authors thank M S C Mazzoni (UFMG) for help with nanotube art work (figure 1). IOM, MAP, FP and AJ acknowledge financial support from the Carbon Nanotube Network, CNPq and FAPEMIG, Brazil.

References

[1] Bachilo S M *et al* 2003 *J. Am. Chem. Soc.* **125** 11186
[2] Fan X *et al* 2000 *Phys. Rev. Lett.* **84** 4621
[3] Grigorian L *et al* 1998 *Phys. Rev. Lett.* **80** 5560
[4] Bendiab N *et al* 2004 *Phys. Rev.* B **69** 195415
[5] Rao A M, Eklund P C, Bandow S, Thess A and Smalley R E 1997 *Nature* **388** 257
[6] Monthiox M 2002 *Carbon* **40** 1809
[7] Fantini C *et al* 2004 *Phys. Rev. Lett.* **93** 147406
[8] O'Connell M J *et al* 2002 *Science* **297** 593
[9] Jorio A *et al* 2005 *Phys. Rev.* B **72** 075207
[10] Eklund P C, Arakawa E T, Zarestky J L, Kamitakahara W A and Mahan G D 1985 *Synth. Met.* **12** 97
[11] Pauling L 1960 *The Nature of the Chemical Bond* (Ithaca, NY: Cornell University Press) p 514